All-angle negative refraction and evanescent wave amplification using one-dimensional metallodielectric photonic crystals

Hocheol Shin[a] and Shanhui Fan
Department of Electrical Engineering, Stanford University, Stanford, California 94305

(Received 30 June 2006; accepted 26 August 2006; published online 9 October 2006)

The authors numerically demonstrate all-angle negative refraction for propagating waves, as well as evanescent wave amplifications, using a one-dimensional photonic crystal consisting of metal-dielectric multilayers. Their structure has uniform surfaces parallel to the object plane and operates at the visible wavelength range. Using realistic material parameters including loss, they design a $Ag-Si_3N_4$ multilayer structure and verified its subwavelength resolution in the image formation process. © *2006 American Institute of Physics*. [DOI: 10.1063/1.2360187]

Media exhibiting negative index or negative refraction effects[1] provide important mechanisms to control electromagnetic waves.[2] Conventional approaches towards creating such media use metamaterials such as dielectric photonic crystals,[3–7] or arrays of metallic resonators,[8–12] both of which are at least two-dimensionally structured at a subwavelength scale. However, due to the increased difficulty to create metamaterials at smaller length scales for operating in the visible or even ultraviolet wavelength range, there have been important recent developments in exploring alternative approaches using structures that have uniform surfaces parallel to the object plane.[13–15]

In this letter, we introduce a negative refraction lens using a one-dimensional metallodielectric photonic crystal, in which each unit cell consists of a metal and a dielectric layer [Fig. 1(a)]. We show that when the plasmonic properties of the metal become prominent, as, for example, in the visible or ultraviolet wavelength range, such a structure provides all-angle negative refraction when light is incident from a positive index medium. Moreover, with proper design, the structure can achieve a resolution beyond the diffraction limit. While such structures, initially studied by Bloemer and Scalora *et al.*[16] as a transparent electrode, were very recently considered for imaging purposes,[17–19] our work explicitly show that all-angle negative refraction for propagating waves and recovery of evanescent components can be simultaneously achieved in such a system.[20]

As a starting point, for simplicity, we use the lossless Drude model to describe the dielectric function of the metal [i.e., $\epsilon_m(\omega)=1-(\omega_p^2/\omega^2)$, where ω_p is the bulk plasma frequency of the metal]. For concreteness, we assume that both metal and dielectric layers are $0.2\lambda_p$ thick, where $\lambda_p \equiv 2\pi c/\omega_p$ (c is the velocity of light in vacuum), and choose the dielectric with the dielectric constant $\epsilon_d=4$. Both metal and dielectric are assumed nonmagnetic (i.e., $\mu=1$).

For the structure, as shown in Fig. 1(a), we numerically calculate the band structure $\omega=\omega(k_x,k_z)$ in the two-dimensional wave vector ($\mathbf{k}$) space, using transfer matrix formalism. All the modes we calculate here have TM polarization that has the magnetic field parallel to the layers. Since the structure is periodic in the x direction and uniform in the z direction, the edges of the first Brillouin zone along the x direction are located at $\pm(\pi/0.4\lambda_p)=\pm 1.25k_p$, where $k_p \equiv 2\pi/\lambda_p$, while k_z extends between $\pm\infty$. We show the projected dispersion relation along the z direction in Fig. 1(b) (Ref. 21) and the dispersion relation $\omega(k_x,k_z=0)$ in Fig. 1(c). The structure supports two bands that both asymptotically

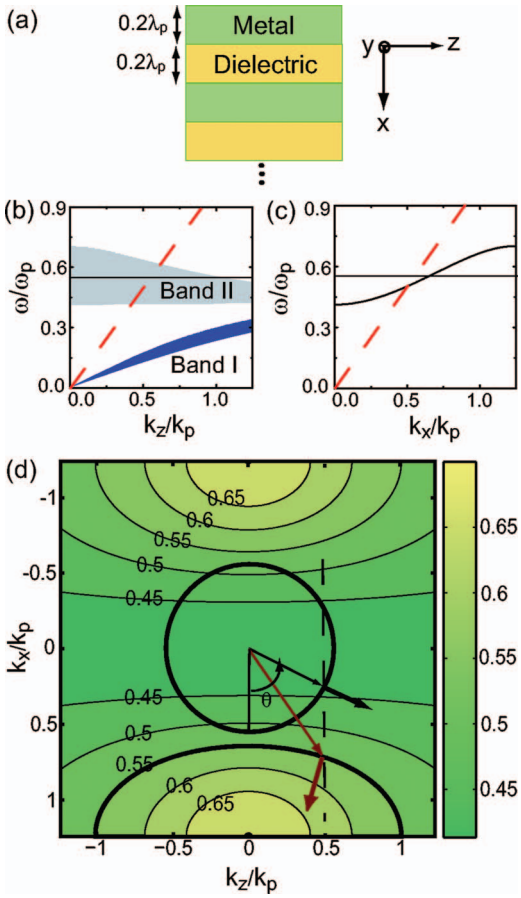

FIG. 1. (Color) (a) Geometry of the metallodielectric photonic crystal structure. (b) A projected band diagram $\omega(k_x,k_z)$ in the z direction and (c) the band diagram $\omega(k_x,k_z=0)$ of the periodic structure in (a). The red dashed lines are the light lines in air and the black horizontal lines indicate the operating frequency of $\omega=0.55\omega_p$. (d) The CFC representation of $\omega(k_x,k_z)$ in the frequency range of the second band, with the contour at $\omega=0.55\omega_p$ highlighted with a thick line. The CFC in air at $\omega=0.55\omega_p$ represented by a black circle is overlaid. For light incident from air onto the crystal at an angle of incidence θ, the thin arrows indicate the wave vectors in air (black) and in the crystal (red), whereas the thick arrows indicate the group velocity directions in air (black) and in the periodic layer region (red). These directions are determined by the procedure as represented by the dashed line, which arises from the conservation of the parallel wave vectors.

[a]Electronic mail: pollini@standford.edu

approach the surface-plasmon frequency of the metal-dielectric interface at large k_z [Fig. 1(b)]. A significant portion of band II lies above the light line. Consequently, externally incident light from air can couple to this band.

To study the refraction properties of light propagation in band II, we plot the corresponding constant frequency contour (CFC) in Fig. 1(d), in the frequency range from $0.45\omega_p$ to $0.65\omega_p$, which is close to the lower and upper edges of this band, respectively. Since the band maximum is located at $\vec{k}_m \equiv (k_x = 1.25k_p, k_z = 0)$, as can be inferred from Figs. 1(b) and 1(c), the CFC's in the frequency range close to $0.65\omega_p$ are of elliptical shapes centered around $\vec{k}_m$, with the size of the contour in the **k** space decreasing with increasing frequencies.

Such a CFC satisfies the condition of all-angle negative refraction for externally incident light from air.[4] As an illustration, we overlay in Fig. 1(d) a CFC of air at $\omega = 0.55\omega_p$ and plot the direction of the refracted beam for light incident from air at an incidence angle θ. The refraction direction, which clearly shows negative refraction behavior, is derived based on the conservation of the parallel wave vector k_z and the fact that the gradient $\nabla_{\mathbf{k}}\omega$ determines the direction of the electromagnetic energy propagation. Also, at this frequency, since the radius of the air CFC is smaller than $k_z^{\max}$, that is, defined as the maximum $|k_z|$ allowed in the photonic crystal, negative refraction occurs for all angles of incidence. For this structure, all-angle negative refraction exists within the entire frequency range of $0.447\omega_p < \omega < 0.615\omega_p$, where the metal-dielectric constant is $-4.00 < \epsilon_m < -1.64$.

We have analyzed similar structures with other geometrical parameters. In general, all-angle negative refraction occurs when the dielectric thickness is less than $\lambda_p\sqrt{\epsilon_d}+1/4\sqrt{\epsilon_d}$, which is closely related to the fact that with the same dielectric thickness a metal-dielectric-metal waveguide exhibits negative group velocity.[22] And the metal layer thickness needs to be less than the skin depth to allow penetration of incident light into the structure.

In addition to focusing the propagating field component, our structure can provide recovery of the evanescent components of an object. For an object in air, the evanescent components have parallel wave vector components $|k_z| > k_0$, where $k_0 = \omega/c$. Using our structure, the evanescent component in the region $k_0 < |k_z| < k_z^{\max}$ can be recovered. In this range of k_z, for the structure with infinite number of periods, there exist propagating Bloch modes (Fig. 1). When the periodic structure is truncated with air, such Bloch modes undergo total internal reflection at the air interface. Therefore, for a slab structure composed of a finite number of metal-dielectric layers, waveguide modes can exist, depending on the thickness of the slab structure.

These waveguide modes provide the mechanism to amplify the optical near field. For our structure with a thickness of 4.5 periods [inset in Fig. 2(a)], using transfer matrix method, we calculate the transmission coefficient through the multilayer structure at different wave vectors k_z at $\omega = 0.55\omega_p$ [Fig. 2(a)]. The transmission coefficient T is defined as the ratio of the complex amplitude of the transmitted wave to the incident wave. The transmission $|T|$ is fairly constant and less than unity in the propagating regime $k_z/k_0 \leqslant 1$ where negative refraction occurs. In the evanescent regime where $k_z/k_0 > 1$, two sharp transmission peaks occur at $k_z = 1.23k_0$ and at $k_z = 1.58k_0$, indicating the existence of waveguide

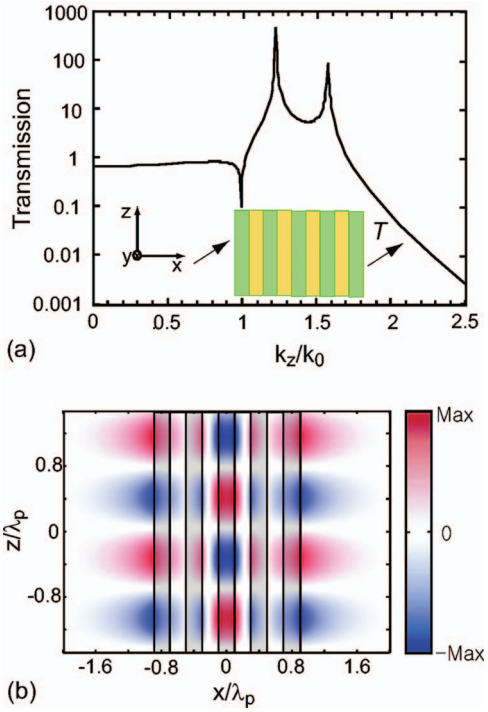

FIG. 2. (Color) (a) Amplitude of the transmission coefficients through a multilayer system as a function of k_z at $\omega = 0.55\omega_p$. The system consists of 4.5 metal-dielectric layers surrounded by air, as shown in the inset, where the green and yellow layers represent metal and dielectric, respectively. (b) The steady-state magnetic field H_y distribution with incident evanescent wave of $k_z = 1.23k_0$ at $\omega = 0.55\omega_p$.

modes. The widths of the peaks are related to the loss in metal and can be arbitrarily small when the loss in metal vanishes, in which case the transmission peak amplitude diverges. The height of the peak greatly exceeds unity, indicating strong amplifications of the optical near field at these wave vector components. Figure 2(b) shows the magnetic field H_y distribution on resonance at $k_z = 1.23k_0$, that is, the signature of the waveguide mode where the field is highly concentrated in the structure. Such amplification due to the presence of the waveguide mode can be effectively used to amplify the decaying evanescent fields from the source, leading to partial recovery of the evanescent field components of the object.[6] Furthermore, it was noted by Luo *et al.*[6] that the use of waveguide mode for subwavelength imaging purpose has better tolerance to deviations from the ideal condition than the surface-plasmon-based mechanism.

The effects of negative refraction for propagating waves and amplification for evanescent waves, as discussed above using an ideal Drude model, also occur in real metal systems with realistic losses, which can be substantial at the optical wavelength ranges. As an example, we consider a structure composed of five layers of Ag and four layers of Si_3N_4. Both Ag and Si_3N_4 layers are 40 nm thick. At the operating wavelength $\lambda = 363.6$ nm, the dielectric constants for Ag and Si_3N_4 are $\epsilon_{Ag} = -2.51 - i0.60$ and $\epsilon_{Si_3N_4} = 4$.[23] Using the transfer matrix method, we calculate the magnetic field H_y distribution both inside and outside of the structure, in the presence of a pointlike object located at 48 nm away in air from the slab surface. The field intensity of the object is Gaussian in the z direction where the full width half maximum (FWHM) is equal to one-tenth of the operating wavelength. The object is formed by a Gaussian-weighted sum of the

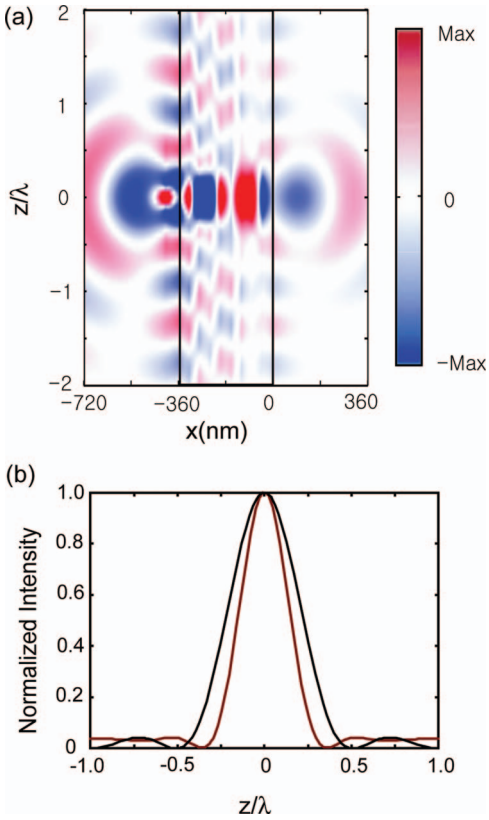

FIG. 3. (Color) (a) Imaging process with a 4.5 period of one-dimensional $Ag-Si_3N_4$ photonic crystal surrounded by air. Plotted here is the magnetic field H_y distribution at the operating wavelength $\lambda=363.6$ nm. (b) The field intensity at the image plane ($x=48$ nm) with the multilayer structure (red) and the diffraction-limited field intensity (black).

plane waves with the parallel wave vector k_z ranging from $-11k_0$ to $11k_0$. To calculate the image, we determine the amplitudes of forward and backward waves for every parallel wave vector component in each layer and superimpose all the plane wave components to obtain the full magnetic field distribution. Figure 3(a) shows the field distribution, which clearly shows an image formed in the opposite side of the structure in air.

To assess the resolution performance of the slab lens, we plot the magnetic field intensity $|H_y|^2$ at the image plane ($x=48$ nm) and compare that image (red) against the diffraction-limited image (black) [Fig. 3(b)]. The diffraction-limited image is calculated by taking only propagating components from the Gaussian object field. The comparison in Fig. 3(b) clearly indicates recovery of the evanescent wave components from the original object field. While the FWHM of the black curve is 0.44λ the FWHM of the red curve is 0.31λ. The same design principle may also be applicable to longer wavelength ranges using other dispersive materials, such as polaritonic media.

This work is in part supported by NSF Grant No. ECS-0134607, AFOSR Grant No. FA9550-04-1-0437, and the Samsung Lee Kun Hee Foundation.

[1]V. G. Veselago, Sov. Phys. Usp. **10**, 509 (1968).
[2]J. B. Pendry, Phys. Rev. Lett. **85**, 3966 (2000).
[3]M. Notomi, Phys. Rev. B **62**, 10696 (2000).
[4]C. Luo, S. G. Johnson, J. D. Joannopoulos, and J. B. Pendry, Phys. Rev. B **65**, 201104 (2002).
[5]E. Cubukcu, K. Aydin, E. Ozbay, S. Foteinopolou, and C. M. Soukoulis, Phys. Rev. Lett. **91**, 207401 (2003).
[6]C. Luo, S. G. Johnson, J. D. Joannopoulos, and J. B. Pendry, Phys. Rev. B **68**, 045115 (2003).
[7]A. Berrier, M. Mulot, M. Swillo, M. Qiu, L. Thylen, A. Talneau, and S. Anand, Phys. Rev. Lett. **93**, 073902 (2004).
[8]J. B. Pendry, A. J. Holden, D. J. Robbins, and W. J. Stewart, IEEE Trans. Microwave Theory Tech. **47**, 2075 (1999).
[9]R. A. Shelby, D. R. Smith, and S. Schultz, Science **292**, 77 (2001).
[10]S. Linden, C. Enkrich, M. Wegener, J. Zhou, T. Koschny, and C. M. Soukoulis, Science **306**, 1351 (2004).
[11]T. Koschny, M. Kafesaki, E. N. Economou, and C. M. Soukoulis, Phys. Rev. Lett. **93**, 107402 (2004).
[12]T. J. Yen, W. J. Padilla, N. Fang, D. C. Vier, D. R. Smith, J. B. Pendry, D. N. Basov, and X. Zhang, Science **303**, 1494 (2004).
[13]V. A. Podolskiy and E. E. Narimanov, Phys. Rev. B **71**, 201101 (2005).
[14]A. Alu and N. Engheta, J. Opt. Soc. Am. B **23**, 571 (2006).
[15]H. Shin and S. Fan, Phys. Rev. Lett. **96**, 073907 (2006).
[16]M. J. Bloemer and M. Scalora, Appl. Phys. Lett. **72**, 1676 (1998).
[17]P. A. Belov and Y. Hao, Phys. Rev. B **73**, 113110 (2006).
[18]S. A. Ramakrishna, J. B. Pendry, M. C. K. Wiltshire, and W. J. Stewart, J. Mod. Opt. **50**, 1419 (2003).
[19]K. J. Webb and M. Yang, Opt. Lett. **31**, 2130 (2006).
[20]We were made aware of an unpublished work by M. Scalora, G. D'Aguanno, N. Akozbek, M. Centini, D. d. Ceglia, M. Cappeddu, N. Mattiucci, J. W. Haus, and M. J. Bloemer (unpublished), http://aps.arxiv.org/abs/physics/0606096 in the final stage of preparing our letter.
[21]E. N. Economou, Phys. Rev. **182**, 539 (1969).
[22]H. Shin, M. F. Yanik, S. Fan, R. Zia, and M. L. Brongersma, Appl. Phys. Lett. **84**, 4421 (2004).
[23]E. D. Palik, *Handbook of Optical Constants of Solids* (Academic, San Diego, 1985).